Multi-instrument observations of the ionospheric response to the 26 December 2019 solar eclipse over Indian and Southeast Asian longitudes

Rajesh Kumar Barad[1], S Sripathi[1], and S. L. England[2]

[1]Indian Institute of Geomagnetism, Plot-5, Sector-18, New Panvel, Navi Mumbai, INDIA
[2]Virginia Polytechnic Institute and State University, Blacksburg, USA

Corresponding Author's Email (Rajesh Kumar Barad):

kumar14mph021@gmail.com/baradrajesh123@gmail.com

Abstract

Here, the impact of the 26 December 2019 solar eclipse on the equatorial and low latitude ionosphere has been investigated using ground and space-based observations over Indian and Southeast Asian longitudes. The high-resolution Ionosonde observations at Tirunelveli, GPS TEC observations from a chain of GPS receivers along and across the eclipse path, TIMED-SABER, and Ionospheric Connection Explorer (ICON) satellites were utilized to investigate the eclipse-induced variations in electron density and thermospheric cooling. We noticed a tremendous increase and decrease in the base height of the F-layer, resembling the nighttime Pre-Reversal Enhancement (PRE). Near the eclipse maximum, a strong blanketing sporadic E layer was observed at Tirunelveli with a top frequency of ~18 MHz for 1 hour and 26 minutes. Satellite traces (STs) and 'U' shaped ionograms were noticed for the first time over Tirunelveli during eclipse maximum and end phases. The 'STs' and 'U' shaped traces indicate the presence of short-period gravity waves or TID type of wave perturbations over the Indian region. A maximum of ~5–7 TECU (30–40%) decrease in TEC is observed on the eclipse day for iisc, hyde, and tiru stations. Periodogram analyses of TEC data showed the presence of wavelike structures with periodicities of 18–24 minutes for different stations. Simultaneous observations from the ICON satellite showed an increase and decrease in hmF2 and NmF2 which matches well with the ionosonde observations from Tirunelveli. The temperature profiles from TIMED-SABER and ICON satellites showed a reduction and enhancement in the lower and upper E regions respectively.

Keywords: Solar eclipse, Gravity waves, Satellite traces, Equatorial ionosphere, Ionosonde observations, GPS TEC observations

Key points:

1. Gravity waves/TID signatures are noticed in the form of satellite traces (STs) and 'U' shaped structures for the first time over Tirunelveli.
2. Periodogram analyses of the TEC data showed the presence of wavelike structures with periodicities of 18–24 minutes at different stations.
3. The temperature profiles showed a reduction and enhancement in the lower and upper E regions respectively.

1. Introduction

A solar eclipse is a rare astronomical event that occurs when the Sun, Moon, and Earth are aligned in a straight line with the moon in between the sun and earth occulting the Sun as well as its radiation by casting a shadow on different parts of the earth. Solar eclipse observation gives a unique opportunity to study the impact of solar radiation on the atmosphere-ionosphere coupled system. The effect of solar eclipses is noticed as a sudden decrease of ionospheric density due to the cutoff of solar ionizing radiation (Mitra et al., 1933). A combination of ground and space-based observations will give an idea about the ionospheric response to the topside and bottom side ionosphere during a solar eclipse. Past studies of the ionospheric response to solar eclipse showed the generation of atmospheric gravity waves in the earth's atmosphere during the eclipse period because of the passage of the Moon's shadow at a supersonic speed (Chimonas and Hines, 1970). Various experimental and modelling techniques have been performed to study the ionospheric response to solar eclipses in the past (Chernogor and Mylovanov, 2020). A Solar eclipse is known to produce changes in the earth's atmosphere and ionosphere. The most common changes are the decrease in electron density, decrease in ion and electron temperature, compositional changes in the ionosphere, plasma movement, and decrease in lower atmospheric temperature. Past solar eclipse studies showed the generation of Travelling Ionospheric Disturbances (TIDs) and gravity waves during solar eclipse using observations. Chimonas and Hines, (1970) have reported for the first time the generation of atmospheric gravity waves during a solar eclipse. Many attempts have been done after this to see the observational evidence (Bertin et al., 1977; Butcher et al., 1979; Davis and Da Rosa, 1970; Ichinose and Ogawa, 1976; Jones et al., 2004). A TID, generated at the shock wave front during the supersonic motion of the Moon's shadow, was detected during eclipse events. The disturbance period and the horizontal projection of the velocity were about 90 minutes and ~680 m/s, respectively. A decrease in 28% of electron density at the F-layer maximum was reported (Afraimovich et al., 2007). Investigation of solar eclipse effects has been done using a number of measuring techniques such as radiosondes, ionosondes, coherent and incoherent scattering radars, geomagnetic field variations, Faraday rotation techniques, and GPS TEC observations (Bamford, 2001; Evans, 1965a, 1965b; Rishbeth, 1968). Verhulst and Stankov, (2020) have studied the effect of eclipse geometry on the geospace environment. According to them, the eclipse effect at the sea level could be different than at different altitudes. This according to them arises due to (a) geometry at the surface and different altitudes, and (b) differences in the emitted radiation at the solar disk and the solar corona. In addition, the differences in the eclipse effect at different altitudes depend on the time and latitude of the eclipse. At the beginning and end of the eclipse, the differences in location and timing of the central eclipse are greater. As the ionosphere is extended vertically, the differences between the central eclipse paths at various altitudes have a significant effect on the location of the maximum TEC depletion.

Patra et al. (2009) have investigated the solar eclipse (11 August 1999) induced low latitude E-region plasma irregularities using Gadanki radar. The solar eclipse creates a night-like situation which then allows the generation of plasma irregularities at multiple layers in the E-region of the ionosphere. They have speculated that these echo layers are associated with long-lived metallic ions that are manifested when ordinary molecular ions get disappeared due to the lack of photoionization. During the eclipse, these ionospheric layers become unstable due to gradient drift instability. Pradipta et al. (2018) have reported ionospheric density irregularities, turbulences, and wave disturbances during the solar eclipse of 21 August 2017 over the North American sector. They have used digisonde and GPS total electron content data to identify different eclipse-induced ionospheric phenomena. The Madrigal TEC, foF2, and foE values showed a decrease of 33–45% during the eclipse. The decrease is in agreement with the model calculations (Huba and Drob, 2017). There is a delay of ~20–30 minutes between the maximum solar obscuration and the occurrence of the minimum value of TEC and foF2, whereas no time delay is observed for minimum foE. The Range-Time-Intensity (RTI) plots reveal the presence of TIDs at F-layer altitudes having a period of ~10 minutes. During maximum obscuration, the spread-F echoes are observed in the mid-latitude sector showing the onset and growth of plasma irregularities in the bottomside of the F region ionosphere. They have reported that Doppler upward velocity of ~100 m/s may be the contributor to the onset and growth of spread-F plasma irregularities via mechanisms like R-T instability or EXB instability.

Recent studies have suggested that gravity waves can be excited both in the lower atmosphere and ionosphere simultaneously due to the presence of the daily variation of the atmosphere-atmosphere system (Šauli et al., 2007). Sometimes other natural phenomena such as geomagnetic storms and tidal variability mask their signatures and hence the difficulty in identifying their sources. Accordingly, the issue of the origin of these waves such as whether they are excited in the stratosphere/troposphere or in situ generated in the ionosphere is still being investigated. During a solar eclipse, the moon's shadow is observed as temporary 'darkness' or 'night' on the earth. This darkness on the earth is extended for longer durations if eclipse magnitude maximizes. Due to this temporary darkness, the ionosphere experiences sudden cooling and the density drops significantly. Solar eclipse produces maximum effects around local noon than evening and morning when solar radiation is found to be significant (Le et al., 2008). Studies suggest that the eclipse effect is stronger in the E and F1 layers than in the F2 layer due to faster recombination in these regions (Bamford, 2001). The impact of the solar eclipses has been studied across many locations, while the passage of eclipses over equatorial regions is of special significance due to its unique geometry where the earth's magnetic field lines are not only horizontal but also perpendicular to the primary zonal electric field that is produced by the lower atmospheric wave dynamics (Sridharan et al., 2002). The equatorial ionosphere is, hence, ideally placed to observe a variety of physical processes that couple the lower atmospheric processes to the upper atmosphere through winds, waves, and tides and modify the primary zonal electric field. The primary electric field again produces the equatorial fountain effect at crest and trough regions under geomagnetically quiet conditions. However, it is believed that the solar eclipse potentially modifies the said quiet-time behaviour temporarily due to sudden modifications in the electric fields, ionization density, and composition due to sudden modifications in the ionization and recombination rates. The daytime conditions could be suddenly reversed to 'nighttime' conditions, and it is possible to cause Pre-Reversal Enhancement (PRE) in the zonal electric field in the daytime that can lead to the development of plasma irregularities and additional ionization layers. It is expected that these plasma density irregularities and additional layers are driven by eclipse-induced density gradients under favourable conditions (Patra et al., 2009). So, it is always exciting to examine the response of the equatorial ionosphere to such rare events as they provide a unique opportunity. The Great American Eclipse of 21 August 2017 has attracted huge attention in the recent past as Americans have witnessed a total solar eclipse for the first time after nearly 100 years. Co-ordinated campaigns were conducted using several scientific instruments across the eclipse path in addition to the modelling studies that produced many interesting aspects such as the passage of bow waves, TIDs, and reduction of E and F region density (Zhang et al., 2017).

Aa et al. (2020) have studied the ionospheric response to the 26 December 2019 solar eclipse using ground-based TEC, EEJ currents, and satellite-based density and temperature measurements. The following results are obtained in their analysis: (a) A reduction in TEC by 30–50%, (b) significant weakening of EEJ currents over the magnetic equator along the path of annularity, and (c) the altitudinal variation of electron density using SWARM and DMSP satellites showed a considerable reduction in the topside ionosphere but enhancement in temperature at 850 km, (d) increase of 20–40% in Equatorial Ionisation Anomaly (EIA) after the eclipse in the noon hours are attributed by the eclipse driven neutral winds and electrodynamics. Similarly, Silwal et al., (2021) have discussed the ionospheric response to 26 December 2019 over Nepal using GNSS TEC observations. They reported a decrease of 20% in TEC as compared to normal days. In this work, a comprehensive study on the 26 December 2019 solar eclipse made of ground and satellite-based observations over India and Southeast Asia is presented with an aim to study the eclipse-induced ionospheric changes and wave perturbations. We have used ionosonde observations from Tirunelveli, India to observe the eclipse-driven modifications in the D, E, and F ionospheric layers. NASA's ICON satellite observations are analysed to see the variations in the thermospheric winds and temperatures, NmF2 and hmf2, and in situ ion parameters. Further, the TEC observations from 8 IGS stations and one SCINDA GPS station located at Tirunelveli are taken to observe changes in TEC values and any gravity wave perturbations in the ionosphere along/across the eclipse path. Magnetic observations from Tirunelveli and Alibag stations are taken into account for Equatorial Electrojet (EEJ) strength. The results obtained on eclipse day indicate prominent changes in thermosphere/ionospheric parameters as compared to adjacent control days.

2. Data and Methodology

2.1 CADI

In this study, we use high-resolution Canadian Digital Advanced Ionosonde (CADI) observations from EGRL (Equatorial Geophysical Research Laboratory), Tirunelveli (8.7°N, 77.8°E geographic). This station is situated close to the eclipse totality path. The ionosonde consists of one delta-type dipole transmitting antenna (peak power 750 W) and four center-fed dipole receiving antenna. The ionosonde has been operated in a high-resolution campaign mode of 2 min to study the eclipse-driven impacts on the ionosphere. The ionosonde was operated at 95 frequencies in a frequency band of 1.5−19 MHz. CADI binary files are processed with "cadi.exe" software to obtain the corresponding ASCII file. These ASCII files are further processed in MATLAB to obtain ionograms and range-time-intensity plots etc.

2.2 Equatorial Electrojet (EEJ)

The Equatorial Electrojet (EEJ) current induces an enhancement in the horizontal component (H-component) of the earth's magnetic field during local noon at the magnetic equator. EEJ strength is calculated by taking the magnetic H-component observations at dip equatorial station Tirunelveli and off equatorial station Alibag which is outside the influence of EEJ current. To compute the EEJ strength at Tirunelveli, first midnight value of H-component is subtracted from each observation at both stations and then the difference between the H-variation from Tirunelveli and Alibag gives the EEJ strength (Rastogi, 1989). In this study, magnetic H-component observations from Alibag and Tirunelveli are taken for 25, 26, and 27 December 2019. From these H-components, we have calculated the EEJ strength over the Indian sector. Note that the time resolution of EEJ is 1 minute.

2.3 Total Electron Content (TEC) Observations

Total Electron Content (TEC) is defined as the total number of electrons lying between the satellite and receiver line of sight of a unit cross-section. GPS satellites send two radiofrequency signals at L1 (1575.42 MHz) and L2 (1227.60 MHz) respectively (Mannucci et al., 1993). TEC can be calculated by considering the dispersive nature of the ionosphere for radio waves. During the propagation of the two dual frequencies radio signals L1 and L2 through the ionosphere, the code signals experience group delay, and the carrier experiences phase advance. The group delay and phase advance are proportional to the electron content along the satellite-receiver line of sight. TEC data is taken from 8 IGS stations (bako, cnmr, guam, guug, hyde, iisc, ntus, pimo) and one SCINDA station (tiru) from Tirunelveli, India.

Figure-1 shows the path of the 26 December 2019 solar eclipse. The three lines in the figure are the north limit, central line, and south limit of the eclipse. In the figure, the cyan triangles are the 8 IGS stations (bako, cnmr, guam, guug, hyde, iisc, ntus, pimo) and one SCINDA station (tiru) from where we have collected GPS TEC data. From the tiru station, high-resolution CADI ionosonde data is obtained.

All the IGS station data have a sampling rate of 30 seconds whereas the SCINDA station data has a sampling rate of 1 minute. For a better comparison of TEC from all the stations, we have taken one minute time average of TEC values from all IGS stations. Not many stations are available close to the eclipse path for this study as the eclipse path lies mostly in the water body. TEC values corresponding to the elevation angle > 20^{o} are considered for this work.

We have used the Savitzky-Golay (S-G) filter of order 5 and frame length 49 to filter TEC data to obtain mainly high-frequency gravity waves from the data. We first filtered the raw data using the S-G filter and then subtracted the filtered data from the raw data to obtain the gravity wave fluctuations. The wave fluctuation is then subjected to Morlet wavelet analysis (Torrence and Compo, 1998).

2.4 ICON and TIMED-SABER Satellite data

NASA's Ionospheric Connection Explorer is a low earth orbiting satellite launched on 10 October 2019. The main aim of the mission is to study the variability in the earth's upper atmosphere/ionosphere by considering the forcing from below as well as above. ICON satellite has four instruments MIGHTI (Michelson Interferometer for Global High-resolution Thermospheric Imaging), EUV (The Extreme Ultraviolet Spectrograph), FUV (The Far Ultra Violet Imaging Spectrograph), and IVM (Ion Velocity Meter) (Immel et al., 2018). MIGHTI gives information about thermospheric wind by observing green and red emissions from oxygen in the 90–300 km altitude range, and temperature by observing infrared emissions from O_2 in the 90–150 km altitude range. ICON-EUV instrument is designed to measure the altitude profile of 61.7 nm and 83.4 nm wavelength emitted by O+ ions. EUV measures the daytime ionospheric density by taking images in the extreme ultraviolet spectrum. IVM measures the velocity, density, and temperature of ions. FUV measures the nighttime Ionospheric density. In this study, temperature information is obtained from MIGHTI, and

NmF2 and hmF2 are taken from EUV, but ion parameters are taken from IVM. The temperature information, and NmF2 and hmF2 are extracted from v05 MGHTI data and v02 EUV data respectively. In addition, we utilize the temperature data from sounding of the atmosphere using Broadband Emission Radiometry (SABER) on-board the Thermosphere Ionosphere Mesosphere Energetics and Dynamics (TIMED) satellite for 25, 26, and 27 December 2019 (Russell et al., 1994). Please note that we mainly use satellite passes closer to the eclipse path to study the cooling effects of the solar eclipse using the temperature profiles in the middle atmosphere using SABER version 2.0 temperature data.

3. Observations

We investigated the background conditions using solar, interplanetary, and geomagnetic observations before we examine the ionospheric response to the solar eclipse. Similarly, we also examined any lower atmospheric events that can mask the eclipse-driven ionospheric perturbation. It is found that all the background conditions remained steady and there is no possible evidence to suggest that eclipse day has geomagnetic/solar influence, and it shows geomagnetically quiet variations.

3.1 CADI Ionosonde Observation

Figure-2(a-c) shows the range-time-intensity (RTI) plots for 25, 26 and 27 December 2019 respectively. The three vertical black lines in figure-2(b) represent the beginning, maximum, and ending of the eclipse phases. It could be observed that the RTI plot on eclipse day is significantly different from the two control days. There are discontinuities in F-region traces after eclipse maximum. The F-region traces have started to appear nearly vertical and then disappeared. It is noteworthy that the presence of strong blanketing sporadic E-layer on the event day has masked the F-layer traces after eclipse maximum.

Figure-3(a-b) shows the temporal variation of foF2 and h'F. The three dashed vertical lines indicate the beginning, maximum, and ending phases of eclipse denoted by the letters B, M, and E respectively. Temporal variation of foF2 is showing some interesting trends during the eclipse period. In the beginning phase of the eclipse, the foF2 value for the eclipse day is ~6 MHz which is slightly greater than the two control day values. As the time progress, foF2 for both 26 and 27 shows an increasing trend and reaches a maximum value of ~6.5 MHz at 3:48 UT. At maximum obscuration, foF2 is decreased to ~6 MHz and again continued to decrease to ~4.9 MHz at 4:02 UT. The figure is showing a gap in foF2 values from 4:48 UT to 6:14

UT on the event day. This is due to the occurrence of strong blanketing Es layer after eclipse maximum and continued even after the end of the eclipse. In the recovery phase of the eclipse, the foF2 has come back to its normal at around 6:14 UT. In this case study, we have observed a strong decrease in foF2 values of 18% from its initial value. Figure-3(b) is showing the abnormal behaviour of h'F on eclipse day. The trend for h'F for eclipse day is quite similar to that of the control day's trend up to3:16 UT. Then it moves up from 199 km to 313 km at 3:36 UT. At the eclipse maximum, it comes down to 230 km. Again, it moves up to an altitude of 453 km at 4:32 UT and comes back to its control day value at 6:28 UT. Such a large enhancement in h'F value is mainly due to two reasons. While one reason could be that the eclipse-induced reduction in the E and F layers of density due to recombination leading to the reflection of radio waves from higher altitudes, the other reason could be due to electrodynamic drift similar to evening Pre-Reversal Enhancement (PRE) caused by eclipse-induced polarization electric field in the E region altitudes.

Figure-3(c-d) shows the temporal variation of foEs and h'Es on eclipse and control days quite similar to foF2 and h'F. It can be observed that Es layer is present on all three days. But on eclipse day after eclipse maximum, the foEs is showing strong enhancement and the foEs value is going upto ~18 MHz at 5:36 UT. For eclipse day, the h'Es is also showing a decreasing trend and reaches a minimum value of 90 km at 5:10 UT. Such a strong decrease in height is mainly due to an increase in Es layer density at lower altitudes.

Figure-4(a-c) depicts the temporal evolution of ionograms from 4:10 UT to 4:18 UT (top to bottom) for all three days. The left panel and right panel correspond to the control days (25^{th} and 27^{th}). The middle panel is for eclipse day. The ionogram echoes for all three days show the presence of Es-layer and F-layer. The shapes of F-traces are quite similar for both the control days. But for the eclipse day, there are kinks in the F1-layer. F2-traces show U-shaped curves. 2F traces are also observed for all three days. Especially, there are extra tilted echoes present between 1F and 2F traces. These kinds of traces are called "Satellite Traces (STs)". The STs are discrete extra traces of range greater than the main F-region trace and are accompanied by the nighttime spread-F phenomenon (McNicol et al., 1956; McNicol and Bowman, 1957). Doublets were observed before spread-F. These doublets arise after reflection from the tilted layer before spread-F (Wright, 1959). The doubling phenomenon is called as the appearance of discrete satellite traces just before the development of Spread-F. STs can be regarded as the precursor for spread-F (Lyon et al., 1961; Rastogi, 1977; Abdu et al., 1981). Such traces are observed for the first time the during the eclipse period. These typical echoes first appear at 4:10 UT and continue for 10 min up to 4:18 UT. It is believed that these types of structures in the ionograms are the signatures of a significant altitude variation of density perturbations and cave-type features in the ionosphere during the eclipse period. Observation and mechanisms of STs have been reported by a few people across the globe. In this work, we would like to address this issue for the first time from a solar eclipse point of view.

3.2 Equatorial Electrojet (EEJ) strength variations

The ground-based magnetic observations at two stations as required for EEJ Strength calculation are obtained from the magnetic observatories located at Tirunelveli and Alibag. To study the E-region current variation during a solar eclipse, we considered the EEJ strength, a current confined to the narrow latitudinal extent centred on the magnetic equator. Detailed variations in ΔH at Tirunelveli/Alibag are shown for comparison. Figure-5(a-d) shows the temporal variation of Dst, ΔH at Alibag and Tirunelveli, and EEJ strength for 25, 26, and 27 December 2019. The three vertical lines are indicating the beginning, maximum, and ending phases of the eclipse. The Dst index is showing quiet time variations for eclipse and control days and hence magnetospheric effects can be neglected. The ΔH at both Alibag and Tirunelveli is showing a slow increase on the eclipse day, unlike normal days. This is due to the modifications in the current system caused by the counter-SQ current system. This counter-SQ current system is generated due to the high-speed movement of the low-pressure system caused by the solar eclipse. On 26 December 2019 EEJ strength is significantly less as compared to 25 and 27 December. At the beginning of the eclipse, the EEJ strength is ~5.3 nT whereas the control days show values of 8–10 nT. As the eclipse progresses the EEJ strength started to increase but the increase is very less as compared to the control days. At the maximum obscuration, the EEJ strength is ~9 nT. The EEJ strength attains a value of ~15 nT at the end of the eclipse. The overall trend of the EEJ strength is that of an increasing trend before eclipse onset, but the increase is drastically curtailed due to the eclipse effect. It is expected that the EEJ strength would decrease in the shadow zone which is noticed here. The SQ current system in the local morning hours is significantly low giving a favourable background condition for the development of a counter-SQ current system which further leads to a decrease in EEJ strength during the eclipse period. Also, the EEJ current which mainly depends on the electron density and electrical conductivity of the equatorial E region gets reduced during the eclipse period. However, we notice enhanced Es layer density during the eclipse period. This can be understood like this: One of the possible mechanisms could be the downward diffusion of plasma towards the lower altitude as well as enhanced wind shears due to gravity waves in the E region during an eclipse can produce strong Es layers but the reduction in the EEJ current could be due to downward drift motion of the E region plasma. So, we believe that even though Es layer density is enhanced due to the dominant role of downward drift motion of plasma, still it can cause a reduction in EEJ currents. This reduction of EEJ current can be seen in our observations. In addition, EEJ strength also showed significant perturbations on eclipse day than on other control days suggesting that significant conductivity variations in the E region on eclipse day were mainly due to neutral wind perturbations induced by gravity waves.

3.3 GPS TEC observations

Figure-6(a-b) depicts the polar plots for iisc and tiru stations along with the eclipse path. Different coloured curves with numbers represent satellite Pseudo Random Numbers (PRNs) crossing or close to eclipse path for iisc and tiru stations. Figure-6(c) shows the daily variation of mean TEC for different stations for eclipse and control days. The mean TEC is obtained using PRNs 10, 31, 12, and 20 for tiru, ntus, guug, guam, cnmr, iisc, hyde, pimo, and bako stations respectively. While the tiru, iisc, and hyde stations show ~5−7 TECU (30-40%) decrease in TEC value as compared to control days, TEC for bako is showing a very small decrease. There is an increase in TEC is observed for pimo. Further ntus, guug, guam and cnmr stations are showing a 4−5 TECU (~30%) decrease from the control day variations. To investigate gravity wave fluctuations on eclipse day, we have analysed PRNs that are crossing/closer to the eclipse path for different stations. After filtering the TEC values using S-G filtering, we performed Morlet wavelet analysis to see the small-scale wave perturbations on the eclipse day. Figure-7 depicts the Morlet wavelet analysis of fluctuations in TEC for different PRNs for different GPS stations along and across the eclipse path. Please note that white gaps in the subplots indicate the non-availability of satellite data for a given PRN. From figure-7, it can be noticed that wavelike structures are present for different stations for particular PRNs. Figure-8(a-c) shows (a) the variation of dominant periods at different stations which are normalized to maximum power (amplitude) across different stations as derived from Figure-7 the TEC fluctuation for PRN-10, 12, 20, and 31 for all the stations on (b) non-eclipse day and (c) eclipse day respectively. Figure-8(a) shows the information about the dominant period of wave oscillation, time corresponding to the wave oscillation, and normalised power (amplitude) of the oscillation with respect to the tiru station where the amplitude of fluctuation is maximum with respect to other stations. Interestingly, it can be seen that the stations closer to the eclipse path are having a higher amplitude in the TEC fluctuations as compared to the stations located away from the eclipse path. This is possibly suggesting that a significant gradient in density closer to the eclipse path may induce higher amplitude TEC fluctuations. Periodicities of the TEC fluctuations lie within the range of ~15–30 minutes with the dominant periods being ~18–24 minutes. Figure-8(b-c) indicates the TEC fluctuation for all the PRNs shown in figure 8(a) for all the stations during control day and eclipse day respectively using the same S-G filtering for comparison. In figure-8 (a-c), the distance in km on the y-axis is calculated using the great circle distance method for all the stations starting from the station "bako" which is the southernmost station. The PRNs of all the stations are stacked from south to north to see gravity wave perturbations and their propagation. It is observed that on eclipse day the TEC fluctuations are dominant compared to control day. On eclipse day enhanced TEC fluctuations as obtained from different PRNs are showing north-south and east-west TEC perturbations induced by eclipse-driven gravity waves which are not present on the control day.

3.4 ICON Satellite and TIMED-SABER Observations

Figure-9(a-b) shows the (a) latitude and longitude variation of NmF2 (MHz) and hmF2 (km) along the ICON satellite path and (b) temporal variation of foF2 (MHz) and hmF2 (km) values as obtained from ICON along the satellite path for 25, 26, and 27 December 2019. Note that foF2 (MHz) is obtained from NmF2 using the following formula: $foF2(MHz) = 9X10^{-3}\sqrt{NmF2\ (cm-3)}$ to compare it with ionosonde foF2 (MHz). The NmF2 and hmF2 from ICON are obtained by using an advanced algorithm to invert the measured OII emission from the EUV spectrograph. The altitude profile of O+ ion concentration is obtained for 150–450 km. Since 95% of the ion concentration in the F-layer is O+ ions, due to charge neutrality the O+ ion density is equivalent to electron density and thus NmF2 and hmF2 can be derived from the measurement (Stephan et al., 2017). From the figure, it can be noticed that there is a decrease in NmF2 (foF2) value on the eclipse day, while the hmF2 value is showing a sharp increase during the eclipse. However, the control days are devoid of such an increase in height. Figure-10(a-d) shows the temperature profile of the upper atmosphere along the ICON satellite path for 25, 26, and 27 December 2019. Also, from Figure-10(a-c) one can clearly observe that there is a large temperature gradient on the eclipse day in the altitude range of ~90–127 km where the lower altitudes show a decrease in temperature, but the upper altitudes show an increase in temperature. Figure-10(d) shows the time average profile of temperature with altitude and its standard deviation on eclipse day and control days. Figure-10(e) shows the temperature difference between the eclipse day and the mean of control days. It can be noticed that there is a decrease of 11 K in temperature in the lower altitude at ~95–98 km whereas an increase of ~17 K in the higher altitudes around ~112–113 km. Next, we show the temperature profiles as obtained from TIMED-SABER. Figure-11(a-b) shows (a) the mean temperature profiles and their standard deviation as obtained from TIMED-SABER for 25, 26, and 27 December 2019 and (b) the difference in the temperature profiles between the eclipse and mean of control days from TIMED-SABER. It can be noticed that there is a decrease of ~40 K in temperature in the lower altitudes ~92 km whereas an increase of ~65 K in temperature is observed at ~102 km. When we compare the ICON and SABER temperature observations, the temperature difference is showing a higher value in SABER as compared to ICON which may possibly depend on different spatial and temporal resolutions and different types of sensors and their sensitivities. One possibility is that SABER is measuring temperature from CO2 whereas ICON is measuring temperature from O2. Given the timescales of the eclipse and the differences in absorption/emission processes for these two molecules. However, the decrease in temperature in the lower altitudes and increase in temperature at higher altitudes is noticed clearly in both the satellites during the eclipse. Such temperature gradients in altitude can generate gravity waves during the eclipse period. We have also checked the in-situ ion parameters obtained from the IVM instrument in the ICON satellite. But these parameters are not showing any changes as compared to eclipse day.

4. Discussions

The following important results are obtained on eclipse day using the analysis presented earlier: 1. Additional ionogram traces like satellite traces (STs) and ‘U’ shaped structures in the ionograms for the first time over Tirunelveli. 2. Periodogram analyses of the TEC data showed the presence of wavelike structures with periodicities of 18–24 minutes at different stations. 3. The temperature profiles showed a reduction and enhancement in the lower and upper E regions respectively during the eclipse. Solar eclipses are known to produce atmospheric gravity waves by localised cooling or heating of the atmosphere (Chimonas and Hines, 1970). Gravity wave-like oscillations are observed after the eclipse recovery phase. Eclipse causes depletion of F-region electron density(Altadill, Gauthier, et al., 2001; Altadill, Solé, et al., 2001). These oscillations can be in-situ generated or propagated from the lower atmosphere. Waves generated in the lower atmosphere due to sudden cooling can propagate to the altitude of the thermosphere-ionosphere system and perturb their dynamics (Fritts and Zhang Luo, 1993). Sridharan et al., (2002) reported changes in electrodynamics of ionospheric E and F-regions caused by the eclipse. Sudden intensification of already existing Es-layer and a significant increase in base height of F-region are also reported. Eclipse also causes E- and F-region plasma irregularities (Patra et al., 2009; Sridharan et al., 2002). During the 26 December 2019 solar eclipse weak Es layer is present before the eclipse starts. However, it can be clearly observed from Figure-2(b) that intensification of Es-layer (Esb-Layer) starts after eclipse maximum at ~04:34 UT and continues for 1 hour 26 mins up to 06:10 UT. No F-region traces are observed during the above period due to the presence of a strong blanketing Es-layer. However, this is not observed on both the control days. Due to the masking of the F layer, we are unable to see any F-region irregularities and density structures in the ionosonde. But the GPS-TEC and scintillation observations are also not showing any L-band scintillations over Tirunelveli. However, as L-band scintillations are caused mainly by intermediate scale size irregularities, we can't rule out whether other scale size irregularities are present or not.

The eclipse induced a sudden drop in the ionization that can affect both E and F regions of the ionosphere which can be seen in our observations. It is believed that this triggers additional electrodynamics due to the development of a sudden low-pressure system that can move east with the Moon's shadow. St.-Maurice et al., (2011) suggested that significant electrodynamics is believed to be developed over the Indian sector during eclipse day. They suggested that the eclipse has produced a counter Sq current and a counter electrojet system that quickly moved eastward as the shadow moved and E region currents were also interrupted due to a decrease in E region conductivity at the centre of the low-pressure system that might cause temporary PRE which possibly, we are seeing a sudden rise in h'F in our observation.

Sridharan et al., (2002) have discussed the effects of the total solar eclipse of 11 Aug 1999 on the electrodynamics of the equatorial E and F regions during sunset hours. Over the Trivandrum sector, the maximum obscuration is ~64%. Observations including VHF backscatter radar of operating frequency 54.95 MHz and HF radar of operating frequency 18 MHz are used to practically analyze effects on the twilight ionosphere. There is a sudden enhancement of weak blanketing Es-layer, enhancement of VHF backscattered returns, increase in h'F immediately following the eclipse, and different spatial and temporal structures in the spread-F irregularity drift velocities as observed by the HF radar. There is a development of gradient instabilities of scale sizes ~2.7 m at steep electron density gradients of the intense blanketing Es layer. The region of 2.7 m irregularities of the E layer is pushed down by ~8 km during the course of the eclipse due to the continuous presence of sharp electron density gradients which is provided by the significantly intense blanketing Es layer. Further, the local and regional background conditions on eclipse day reduce the E region loading of F region dynamo giving rise to the increase in post-sunset F-region heights as compared to the control day. In our observation, we are seeing a strong enhancement in F-region height that may be due to the eclipse creating a nighttime situation where the F-layer height goes up and then comes down.

Nayak et al. (2012) have investigated the effects of the annular solar eclipse (15 January 2010) on the ionization of E and F layers of the equatorial ionosphere over Tirunelveli using CADI Ionosonde when the maximum obscuration is ~84% in the afternoon. There is a change in the Es layer with time during eclipse day. The Es layer continues to become weaker from the onset to the end of the eclipse. They have also reported the intensification of blanketing Es layer and then there is a decreasing trend and finally gets disappeared. We also investigated the 15 January 2010 solar eclipse effects on the atmosphere-ionosphere system. The results suggest that there is a strong reduction of F1 density (~33%) but F2 layer density is devoid of such reduction on eclipse day. But we have seen a decrease of ~18% in the foF2 for the 26 December 2019 solar eclipse. Strong blanketing Es-layer is observed for 1 hour and 26 minutes. Such a strong Esb has not observed for the 15 January 2010 eclipse event.

Gravity wave generation by the solar eclipse is proposed by Chimonas and Hines, (1970) which is verified by Davis and Da Rosa, (1970) using experiments. But few researchers suggest that the gravity waves as seen in the ionosphere could be due to the sudden cooling of the ionosphere itself (Altadill, Solé, et al., 2001). Beer (1973), on the other hand, has suggested that the sources for these gravity waves could be in the regions of molecular oxygen above 90 km, the ozone layer at 50 km that absorb solar UV radiation, and the surface/ground and tropospheric altitude where carbon dioxide and water vapour can absorb the energy and re-radiate from the surface due to solar eclipses. From NASA's ICON satellite observation, we observed the change in upper atmospheric temperature during the eclipse. The temperature profile shows a large gradient in the altitude range of ~90–127 km. The temperature profiles using the TIMED-SABER also showed a significant reduction in the lower altitudes but an increase at higher altitudes similar to the ICON satellite. Accordingly, the temperature profiles from both the TIMED-SABER and ICON satellites suggest a reduction and enhancement in the lower and upper E regions respectively leading to the sudden inversions which can excite atmospheric gravity waves during the solar eclipse. To identify gravity wave activity along the eclipse path, usually, TEC observations across/along the eclipse path were investigated (Maurya et al., 2020; Nayak and Yiğit, 2018). We have examined 9 stations to see the gravity wave propagation in the TEC data. Most of the stations show a clear decrease in TEC values after the eclipse onset then reach a minimum around the eclipse maximum and then gradually recover. Similar behaviour was predicted in the work by Huba and Drob, (2017). In the observations, however, the decrease may not perfectly coincide with the start of the eclipse. The TEC attains a minimum, not at the maximum eclipse but a few minutes afterward. Instead, there seems to be a time lag of ~2–11 minutes for iisc, tiru, and hyde stations. Other stations like ntus, guug, guam, guug show a time lag of 40–50 minutes. These time lags are mainly dependent on the local background ionosphere. Stations in the local morning sector are showing a small time lag as compared to afternoon/evening sector stations. The reason for such a lag comes due to the delayed response of the F_2 layer to the eclipse. TEC depletion of ~5–7 TECU (30–40 %) is observed during the eclipse maximum. Aa et al. (2020) and Silwal et al. (2021) have shown a TEC depletion of 20–50% for the 26 December 2019 solar eclipse. In the present study, we have noticed the presence of gravity wave-type of oscillations with higher amplitude at stations close to the eclipse path. As we move away from the eclipse path the amplitude decreases. This is in good agreement with the prediction made by Chimonas and Hines, (1970). Few results suggest that eclipse-induced strong lunar tidal forces are dominant during eclipses and can possibly produce counter electrojet (Panda et al., 2015; Vyas and Sunda, 2012). The presence of gravity wave-like oscillations with periods in the range of 20–90 minutes have also been noticed in the GPS TEC observations in the path of totality and away from the totality during the Great American Eclipse on 21 August 2017 (Nayak and Yiğit, 2018). However, their observations also suggest that the gravity wave amplitudes are higher at the locations that are closer to the totality than away from the totality. Altadill and Solé, et al. (2001) have suggested that since the transition region between E and F regions is significantly affected by the photoionization and dynamics, it is possible that this region could be prone to more turbulence and can produce gravity wave oscillations. Since we noticed strong Es layers, the presence of turbulent structures and gravity waves in the F layer could not be recorded in ionosonde. Accordingly, we don't see any density irregularities in our observations except evidence for strong blanketing Es layers. GPS TEC and scintillation observations do confirm that there are no L band scintillations at the time of eclipse onset. Since Es layers are excited by strong winds and wind shears which are possible during eclipse and CEJ events, the presence of strong Es layers in our case does support that there were strong winds and wind shears with altitude over the equatorial region due to sudden local cooling of the atmosphere/ionosphere.

Manju et al. (2014) have investigated the gravity wave signatures during the solar eclipse of 15 January 2010 in the ionosphere-thermosphere region over Trivandrum. Due to solar obscuration, there is a sudden cooling during solar eclipse gives rise to a change in pressure and hence generates internal gravity waves of period 30-100 minutes. This periodicity is obtained from the spectral analysis of the NmF1 and NmF2 time series. The vertical wavelength of the eclipse-induced gravity waves is found to be 2km by using the rocket-borne horizontal wind measurement and electron density of the E layer. There is upward wave propagation in the region between F1 and F2 peak and also a downward propagation in the height range of about 110 km revealing the source is in between these altitudes. Strong backscattered signals as obtained from HF radar at Thumba specify the presence of blanketing Es-type irregularities during the maximum solar obscuration.

In our observation due to the presence of a strong blanketing Es-layer, there is a gap in h'F and foF2 observations. One of the possible reasons for such a strong Es layer during an eclipse in the present case could be related to the downward motion of higher altitude density to the E region which can increase the E region density. Another reason could be that there were strong winds and wind shears were present which could have increased Es layer density. Since EEJ is significantly reduced on the eclipse day than on the control days which may favour the downward motion resulting in enhanced Es-layer at the dip equator. Additional forces such as vertical winds and horizontal shears of horizontal winds could play an important role in the Es-layer formation (Reddy and Devasia, 1973; Raghavarao et al., 1987). Sridharan et al., (2002) have suggested that vertical winds could play a significant role at the equatorial locations. The vertical winds could be of gravity wave origin. Since we have noticed strong gravity wave activity on eclipse day over Tirunelveli, it is believed that the eclipse-induced large circulation pattern due to temperature/pressure changes might produce such vertical winds. In the absence of supporting wind information, we only speculate that this could be the mechanism for the formation of the Es-layer during the solar eclipse of 26 December 2019. Also, the strong increase in F-layer height and occurrence of ‘STs’ and ‘U’ shaped ionograms at the same time may be indicating significant modifications in the density and wavy structures in the ionosphere and also possible downward diffusion of density to lower altitudes. The gravity waves induced by the eclipse in the Mesosphere Lower Thermosphere (MLT) region can propagate to E and F regions and can manifest as TIDs through collisions with ionized species. The ‘U’ shaped structures in the ionosphere during eclipse accordingly suggest that significant dynamics and electrodynamics were developed in the E and F1 layers over Tirunelveli. The ‘U’ shaped ionograms are mainly detected whenever F layer density undergoes modulations, wind shears, gravity waves, or TIDs perturbations. However, STs usually can be regarded as the precursors for spread-F in the nighttime. In our observations, STs are observed for the first time on eclipse day, and they appeared mainly during and after the eclipse period. On eclipse day due to the presence of a strong blanketing Es layer, we do not have the information about the F-layer to see the F-layer structures after the occurrence of STs. It appears that STs also appear in ionograms without the further development of any spread-F. It can arise due to reflections from tilts in the bottomside of the F-region of the ionosphere. Tsunoda, (2008) has reported the presence of satellite traces in ionograms as a signature of large-scale wave structures (LSWS) and a precursor for impending equatorial spread F. Satellite traces are manifestations of reflections from isodensity contours within the crest of an LSWS. Ionogram traces depend on the exact position of the structure in the isodensity contours and its position with respect to ionosonde. It is noteworthy that the satellite traces appearing after the eclipse end is also not associated with any kind of equatorial spread-F. We believe that these F-layer traces could be mainly due to the eclipse-driven gravity wave induced tilts in the bottom of the F-region of the ionosphere. We surmise that the unusual variations in the base height of the F-Layer can give rise to such tilts in the bottom of the ionospheric F-region and hence can be observed as STs. Narayanan et al., (2014) examined ionosonde data from EGRL, Tirunelveli and suggested that not all STs will lead to ESF which also matches with our result. Lynn et al.(2011) have observed plasma bubbles using ionosonde and airglow imaging simultaneously. Tree-like structures are present in airglow observations. Ionosonde range-time analysis shows the presence of off-angle echoes (STs). Both the results complemented each other. However, in our case, we don’t have such simultaneous optical observations to confirm the presence of any plasma depletions or irregularities developed during the eclipse period. But GPS TEC and scintillation observations indicate the presence of no scintillations or F-layer density irregularities. Thus, these STs could be regarded as a manifestation of eclipse-driven tilts in the bottom side of the F-layer and these STs are regarded as direct signatures of LSWS. This probably indicates the presence of strong wave activity during the eclipse period. Also, no such satellite traces are reported earlier in any eclipse event. We have also examined previous eclipse events over Tirunelveli using CADI and found that no such STs are detected during eclipse events. Hence, this is a unique observation during a solar eclipse. The underlying physical mechanism is still an open question which we would like to address in the future.

5. Summary and conclusions

In this study, we have analysed the high-resolution CADI ionosonde data, GPS-TEC observations from 9 stations, EEJ data, NASA's ICON and TIMED-SABER satellite observations to see the effect of the 26 December 2019 solar eclipse on the atmosphere-ionosphere system. Results suggest that solar eclipse can significantly perturb the atmosphere-ionosphere system. The virtual height of the F-layer showed tremendous variation during the maximum and decay phase as compared to the growth phase. The results suggest a reduction of ~18% in the foF2 on the eclipse day than on control days. The occurrence of strong blanketing sporadic E-layer is observed for 1 hour and 26 minutes. 'U' shaped ionogram structures and additional traces between 1F and 2F traces are unique features noticed in the ionograms for the first time during an eclipse. EEJ strength showed its significant reduction along with wavy features on the eclipse day, but no CEJ is observed. This may be due to the sudden changes or modifications in the E-region conductivity. Nearly 5–7 TECU (30–40%) decrease in TEC is noticed at tiru, hyde, and iisc stations. GPS-TEC observations indicate the propagation of wave-like structures during the eclipse period possibly excited due to the sudden inversions and changes in the temperature of the upper atmosphere. Observation from NASA's ICON satellite showed a large gradient in the temperature profile of the earth's atmosphere which might be the reason behind the excitation of such waves in the upper atmosphere. The NmF2 and hmF2 obtained from the EUV instrument of the ICON satellite indicate a similar trend of height enhancement and density depletion along the satellite path as observed from CADI, Tirunelveli. The temperature profiles from both the TIMED-SABER and ICON satellites showed a reduction and enhancement in the lower and upper E regions respectively during the eclipse.

Acknowledgement

The work presented in this paper is through financial support from the institute project 'NECLAS'. We are thankful to the Director for his kind support and necessary help. We also wish to thank Mr. Selvaraj and Mr. Emperumal, IIG for conducting the eclipse field campaign at Tirunelveli to collect high-resolution ionosonde measurements and make the data available for the investigations presented here. We also wish to thank Dr. Keith Groves, Boston College, USA for providing the SCINDA GPS receiver and its data for the studies presented here. We are thankful to the technical staff of the geomagnetic data collection and processing group at IIG for providing us with the EEJ strength data for the studies presented here. We would like to thank the ICON team for providing data for this study. ICON data are processed in the ICON Science Data Center at UCB and available at https://icon.ssl.berkeley.edu/Data and NASA's Space Physics Data Facility at https://spdf.gsfc.nasa.gov/.We thank the SABER team for providing SABER data (http://saber.gats-Inc.com/data.php) presented here. The observational data of ionosonde presented here can be accessed at https://doi.org/10.5281/zenodo.7009949.

References

Aa, E., Zhang, S. R., Erickson, P. J., Goncharenko, L. P., Coster, A. J., Jonah, O. F., et al. (2020). Coordinated Ground-Based and Space-Borne Observations of Ionospheric Response to the Annular Solar Eclipse on 26 December 2019. *Journal of Geophysical Research: Space Physics*, *125*(11), 1–17. https://doi.org/10.1029/2020JA028296

Abdu, M. A., Batista, I. S., & Bittencourt, J. A. (1981). Some characteristics of spread F at the magnetic equatorial station Fortaleza. *Journal of Geophysical Research*, *86*(A8), 6836. https://doi.org/10.1029/ja086ia08p06836

Afraimovich, E. L., Voeykov, S. V., Perevalova, N. P., Vodyannikov, V. V., Gordienko, G. I., Litvinov, Y. G., & Yakovets, A. F. (2007). Ionospheric effects of the March 29, 2006, solar eclipse over Kazakhstan. Geomagnetism and Aeronomy, 47(4), 461–469. https://doi.org/10.1134/S0016793207040068

Altadill, D., Gauthier, F., Vila, P., Sole, J. G., Miro, G., & Berranger, R. (2001). The 11.08.1999 solar eclipse and the ionosphere: a search for the distant bow-wave. *Journal of Atmospheric and Solar-Terrestrial Physics*, *63*(9), 925–930. https://doi.org/10.1016/s1364-6826(00)00204-2

Altadill, D., Solé, J. G., & Apostolov, E. M. (2001). Vertical structure of a gravity wave like oscillation in the ionosphere generated by the solar eclipse of August 11, 1999. *Journal of Geophysical Research: Space Physics*, *106*(A10), 21419–21428. https://doi.org/10.1029/2001ja900069

Bamford, R. A. (2001). The effect of the 1999 total solar eclipse on the ionosphere. *Physics and Chemistry of the Earth, Part C: Solar, Terrestrial and Planetary Science*, *26*(5), 373–377. https://doi.org/10.1016/S1464-1917(01)00016-2

Beer, T. (1973). Supersonic generation of atmospheric waves. *Nature*, *242*(5392), 34. https://doi.org/10.1038/242034a0

Bertin, F., Hughes, K. A., & Kersley, L. (1977). Atmospheric waves induced by the solar eclipse of 30 June 1973. *Journal of Atmospheric and Terrestrial Physics*, *39*(4), 457–461. https://doi.org/10.1016/0021-9169(77)90153-2

Butcher, E. C., Downing, A. M., & Cole, K. D. (1979). Wavelike variations in the F-region in the path of totality of the eclipseb of 23 October 1976. *Journal of Atmospheric and Terrestrial Physics*, *41*(5), 439–444. https://doi.org/10.1016/0021-9169(79)90068-0

Chernogor, L. F., & Mylovanov, Y. B. (2020). Ionospheric Effects of the August 11, 2018, Solar Eclipse over the People's Republic of China. *Kinematics and Physics of Celestial Bodies*, *36*(6), 274–290. https://doi.org/10.3103/S0884591320060021

Chimonas, G., & Hines, C. O. (1970). Atmospheric gravity waves induced by a solar eclipse. *Journal of Geophysical Research*, *75*(4), 875–875. https://doi.org/10.1029/JA075i004p00875

Davis, M. J., & Da Rosa, A. V. (1970). Possible detection of atmospheric gravity waves generated by the solar eclipse. *Nature*, *226*(5251), 1123. https://doi.org/10.1038/2261123a0

Evans, J. V. (1965a). An F region eclipse . *Journal of Geophysical Research*, *70*(1), 131–142. https://doi.org/10.1029/jz070i001p00131

Evans, J. V. (1965b). On the behavior of *ƒ* 0 F 2 during solar eclipses. *Journal of Geophysical Research*, *70*(3), 733–738. https://doi.org/10.1029/JZ070i003p00733

Fritts, D. C., & Zhang Luo. (1993). Gravity wave forcing in the middle atmosphere due to reduced ozone heating during a solar eclipse. *Journal of Geophysical Research*, *98*(D2), 3011–3021. https://doi.org/10.1029/92JD02391

Huba, J. D., & Drob, D. (2017). SAMI3 prediction of the impact of the 21 August 2017 total solar eclipse on the ionosphere/plasmasphere system. *Geophysical Research Letters*, *44*(12), 5928–5935. https://doi.org/10.1002/2017GL073549

Ichinose, T., & Ogawa, T. (1976). the total electron content was observed by above Doppler shifts in the radio wave propagated in the, *81*(13), 2401–2404.

Immel, T. J., England, S. L., Mende, S. B., Heelis, R. A., Englert, C. R., Edelstein, J., et al. (2018). *The Ionospheric Connection Explorer Mission: Mission Goals and Design*. *Space Science Reviews* (Vol. 214). Springer Science+Business Media B.V., part of Springer Nature. https://doi.org/10.1007/s11214-017-0449-2

Jones, T. B., Wright, D. M., Milner, J., Yeoman, T. K., Reid, T., Chapman, P. J., & Senior, A. (2004). The detection of atmospheric waves produced by the total solar eclipse of 11 August 1999. *Journal of Atmospheric and Solar-Terrestrial Physics*, *66*(5), 363–374. https://doi.org/10.1016/j.jastp.2004.01.029

Le, H., Liu, L., Yue, X., & Wan, W. (2008). The midlatitude F2 layer during solar eclipses: Observations and modeling. *Journal of Geophysical Research: Space Physics*, *113*(8), 1–10. https://doi.org/10.1029/2007JA013012

Lynn, K. J. W., Otsuka, Y., & Shiokawa, K. (2011). Simultaneous observations at Darwin of equatorial bubbles by ionosonde-based range/time displays and airglow imaging. *Geophysical Research Letters*, *38*(23), 2–5. https://doi.org/10.1029/2011GL049856

Lyon, A. J., Skinner, N. J., & Wright, R. W. (1961). Equatorial spread-F at Ibadan, Nigeria. *Journal of Atmospheric and Terrestrial Physics*, *21*(2–3). https://doi.org/10.1016/0021-9169(61)90104-0Manju, G., Madhav Haridas, M. K., Ramkumar, G., Pant, T. K., Sridharan, R., & Sreelatha, P. (2014). Gravity wave signatures in the dip equatorial ionosphere-thermosphere system during the annular solar eclipse of 15 January 2010. *Journal of Geophysical Research: Space Physics*, *119*(6), 4929–4937. https://doi.org/10.1002/2014JA019865

Mannucci, A. J., Wilson, B. D., & Edwards, C. D. (1993). A New Method for Monitoring the Earth's Ionospheric Total Electron Content Using the GPS Global Network. Proceedings of the 6th International Technical Meeting of the Satellite Division of The Institute of Navigation (ION GPS 1993), Salt Lake City, UT, 1323-1332. https://www.ion.org/publications/abstract.cfm?articleID=4319

Maurya, A. K., Shrivastava, M. N., & Kumar, K. N. (2020). Ionospheric monitoring with the Chilean GPS eyeball during the South American total solar eclipse on 2nd July 2019. Scientific Reports, 10(1), 1–10. https://doi.org/10.1038/s41598-020-75986-7

McNicol, R. W., H. C. Webster, and G. G. Bowman (1956), A study of "Spread-F" ionospheric echoes at night at Brisbane: Range spreading (Experimental), *Aust. J. Phys.*, 9, 247–271, doi:10.1071/PH560247.

McNicol, R. W. E., and G. G. Bowman (1957), Latitude Variations of Frequency of Occurrence of "Spread-F" Satellite Traces, Australian J. of Physics, 10, 588–590.

MITRA, S. K., RAKSHIT, H., SYAM, P., & GHOSE, B. N. (1933). Effect of the Solar Eclipse on the Ionosphere. Nature, 132(3333), 442–443. https://doi.org/10.1038/132442a0

Narayanan, V. L., Sau, S., Gurubaran, S., Shiokawa, K., Balan, N., Emperumal, K., & Sripathi, S. (2014). A statistical study of satellite traces and evolution of equatorial spread F Space science. *Earth, Planets and Space*, *66*(1), 1–13. https://doi.org/10.1186/s40623-014-0160-4

Nayak, C., & Yiğit, E. (2018). GPS-TEC Observation of Gravity Waves Generated in the Ionosphere During 21 August 2017 Total Solar Eclipse. *Journal of Geophysical Research: Space Physics*, *123*(1), 725–738. https://doi.org/10.1002/2017JA024845

Nayak, C. K., Tiwari, D., Emperumal, K., & Bhattacharyya, A. (2012). The equatorial ionospheric response over Tirunelveli to the 15 January 2010 annular solar eclipse: Observations. *Annales Geophysicae*, *30*(9), 1371–1377. https://doi.org/10.5194/angeo-30-1371-2012

Panda, S. K., Gedam, S. S., Rajaram, G., Sripathi, S., & Bhaskar, A. (2015). Impact of the 15 January 2010 annular solar eclipse on the equatorial and low latitude ionosphere over the Indian region. *Journal of Atmospheric and Solar-Terrestrial Physics*, *135*, 181–191. https://doi.org/10.1016/j.jastp.2015.11.004

Patra, A. K., Choudhary, R. K., & St-Maurice, J. P. (2009). Solar eclipse-induced E-region plasma irregularities observed by the Gadanki radar. *Geophysical Research Letters*, *36*(13). https://doi.org/10.1029/2009GL038669

Pradipta, R., Yizengaw, E., & Doherty, P. (2018). Ionospheric Density Irregularities, Turbulence, and Wave Disturbances During the Total Solar Eclipse Over North America on 21 August 2017. *Geophysical Research Letters*, *45*(16), 7909–7917. https://doi.org/10.1029/2018GL079383

Raghavarao, R., Gupta, S. P., Sekar, R., Narayanan, R., Desai, J. N., Sridharan, R., et al. (1987). In situ measurements of winds, electric fields and electron densities at the onset of equatorial spread-F. Journal of Atmospheric and Terrestrial Physics, 49(5), 485–492. https://doi.org/10.1016/0021-9169(87)90042-0

Rastogi, R.G. (1977) Equatorial range spread *F* and high multiple echoes from the *F* region. *Proc. Indian Acad. Sci., 85*, 230–235. https://doi.org/10.1007/BF03049485

Rastogi, R. G., 1989. The equatorial electrojet: magnetic and ionospheric effects. In: Jacobs, J. (Ed.), Geomagnetism, vol. 3. Academic Press, SanDiego, CA, pp. 461–525.

Reddy, C. A., & Devasia, C. V. (1973). Formation of blanketing sporadic E-layers at the magnetic equator due to horizontal wind shears. Planetary and Space Science, 21(5). https://doi.org/10.1016/0032-0633(73)90098-6

Rishbeth, H. (1968). Solar eclipses and ionospheric theory. *Space Science Reviews*, *8*(4), 543–554. https://doi.org/10.1007/BF00175006

Šauli, P., Roux, S. G., Abry, P., & Boška, J. (2007). Acoustic-gravity waves during solar eclipses: Detection and characterization using wavelet transforms. *Journal of Atmospheric and Solar-Terrestrial Physics*, *69*(17–18), 2465–2484. https://doi.org/10.1016/j.jastp.2007.06.012

Silwal, A., Gautam, S. P., Chapagain, N. P., Karki, M., Poudel, P., Ghimire, B. D., et al. (2021). Ionospheric Response over Nepal during the 26 December 2019 Solar Eclipse. *Journal of Nepal Physical Society*, *7*(1), 25–30. https://doi.org/10.3126/jnphyssoc.v7i1.36970

Sridharan, R., Devasia, C. V, Jyoti, N., Tiwari, D., Viswanathan, K. S., & Subbarao, K. S. V.

(2002). Effects of solar eclipse on the electrodynamical processes of the equatorial ionosphere: A case study during 11 August 1999 dusk time total solar eclipse over India. *Annales Geophysicae*, *20*(12), 1977–1985. https://doi.org/10.5194/angeo-20-1977-2002

St.-Maurice, J.-P., Ambili, K. M., & Choudhary, R. K. (2011). Local electrodynamics of a solar eclipse at the magnetic equator in the early afternoon hours. *Geophysical Research Letters*, *38*(4), n/a-n/a. https://doi.org/10.1029/2010GL046085

Stephan, A. W., Korpela, E. J., Sirk, M. M., England, S. L., & Immel, T. J. (2017). Daytime Ionosphere Retrieval Algorithm for the Ionospheric Connection Explorer (ICON). *Space Science Reviews*, *212*(1–2), 645–654. https://doi.org/10.1007/s11214-017-0385-1

Torrence, C., & Compo, G. P. (1998). A Practical Guide to Wavelet Analysis. *Bulletin of the American Meteorological Society*, *79*(1), 61–78. https://doi.org/10.1175/1520-0477(1998)079<0061:APGTWA>2.0.CO;2

Tsunoda, R. T. (2008). Satellite traces: An ionogram signature for large-scale wave structure and a precursor for equatorial spread F. *Geophysical Research Letters*, *35*(20), 2–5. https://doi.org/10.1029/2008GL035706

Verhulst, T. G. W., & Stankov, S. M. (2020). Height Dependency of Solar Eclipse Effects: The Ionospheric Perspective. *Journal of Geophysical Research: Space Physics*, *125*(7), 1–20. https://doi.org/10.1029/2020JA028088

Vyas, B. M., & Sunda, S. (2012). The solar eclipse and its associated ionospheric TEC variations over Indian stations on January 15 , 2010. *Advances in Space Research*, *49*(3), 546–555. https://doi.org/10.1016/j.asr.2011.11.009

Wright, R. W. H. (1959). Geomorphology of spread F and characteristics of equatorial spread F. *Journal of Geophysical Research*, *64*(12), 2203–2207. https://doi.org/10.1029/jz064i012p02203Zhang, S. R., Erickson, P. J., Goncharenko, L. P., Coster, A. J., Rideout, W., & Vierinen, J. (2017). Ionospheric Bow Waves and Perturbations Induced by the 21 August 2017 Solar Eclipse. *Geophysical Research Letters*, *44*(24), 12,067-12,073. https://doi.org/10.1002/2017GL076054

Figure captions

Figure-1 shows the path of the 26 December 2019 solar eclipse. The three lines in the figure are the north limit, central line, and south limit of the eclipse. In the figure, the cyan triangles are the 8 IGS stations (bako, cnmr, guam, guug, hyde, iisc, ntus, pimo) and one SCINDA station (tiru) from where we have collected GPS TEC data. From the tiru station high-resolution CADI ionosonde data is obtained.

Figure-2(a-c) shows the range-time-intensity (RTI) plots for 25, 26 and 27 December 2019 respectively. The three vertical black lines in figure-2(b) are representing the beginning, maximum, and ending of the eclipse.

Figure-3(a-b) shows the temporal variation of foF2 and h'F. The three dashed vertical lines indicate the beginning, maximum, and ending phase of the eclipse denoted by the letters B, M, and E respectively. Figure-3(c-d) shows the foEs and h'Es variation on eclipse and control days.

Figure-4(a-c) depicts the temporal evolution of ionograms from 4:10 UT to 4:18 UT (top to bottom) for all three days. The left panel and right panel correspond to the control days (25th and 27th).

Figure-5(a-d) shows the temporal variation of (a) Dst index, (b) ΔH at Alibag, (c) ΔH at Tirunelveli, and (d) EEJ strength on 25, 26, and 27 Dec 2019. The three vertical lines indicate the beginning, maximum, and ending phases of the eclipse.

Figure-6(a-c) depicts (a-b) the polar plots for iisc and tiru stations along with eclipse path. Different coloured curves with numbers represent Pseudo Random Numbers (PRNs) crossing or close to eclipse path for iisc and tiru station, (c) variation of mean TEC for different stations on eclipse and control days.

Figure-7 depicts the Morlet wavelet analysis of fluctuations in TEC for different PRNs for different GPS stations along and across the eclipse path.

Figure-8(a-c) shows (a) the variation of dominant periods at different stations which are normalized to maximum power (amplitude) across different stations as derived from Figure-7, the TEC fluctuations for PRN-10, 12, 20, and 31 for all the stations on (b) non-eclipse day, and (c) eclipse day respectively.

Figure-9(a-b) shows the (a) latitude-longitude variation of NmF2 and hmF2 using ICON satellite paths on 25, 26, and 27 December 2019 and (b) temporal variation of foF2 (MHz) and hmF2 (km) values along the satellite paths for 25, 26, and 27 December 2019. Please note that $foF2(MHz) = 9X10^{-3}\sqrt{NmF2\ (cm-3)}$

Figure-10(a-c) show the contour maps of time-altitude variation of temperature profiles of the upper atmosphere along the ICON satellite path on 25, 26, and 27 December 2019 respectively and their (d) altitude variation of mean temperature profiles on 25, 26, and 27 December 2019 (e) the temperature difference between eclipse day and mean of control days.

Figure-11(a-b) shows (a) the mean temperature profiles and their standard deviation as obtained from TIMED-SABER for 25, 26, and 27 December 2019 and (b) the difference in the temperature profiles between the eclipse and mean of control days from TIMED-SABER.

Figure1.

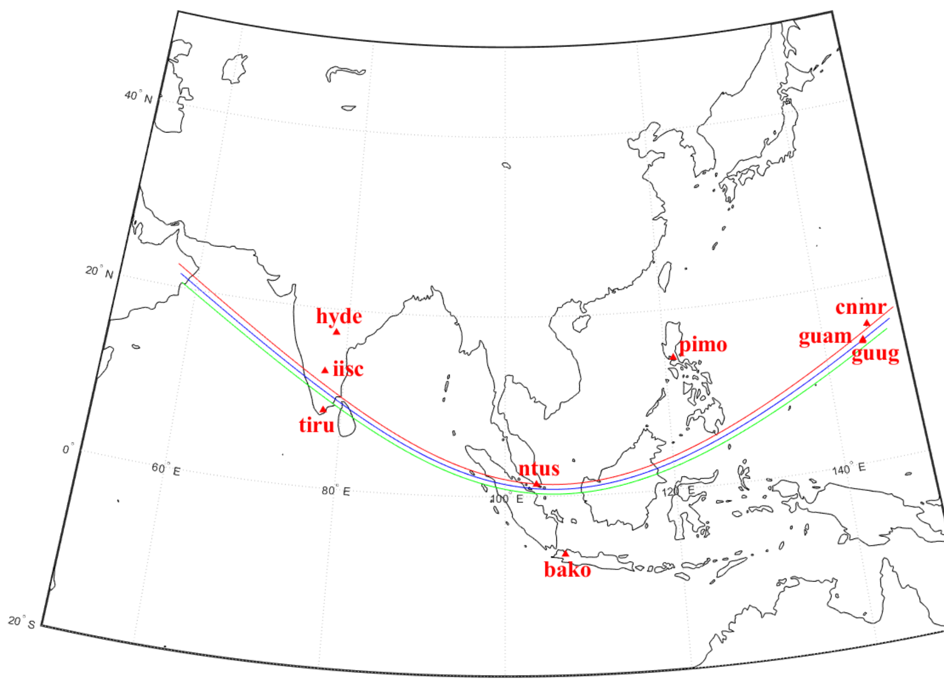
40° N
20° N
0°
20° S
60° E
80° E
100° E
120° E
140° E
hyde
iisc
tiru
ntus
bako
pimo
cnmr
guam
guug

Figure-2(a-c).

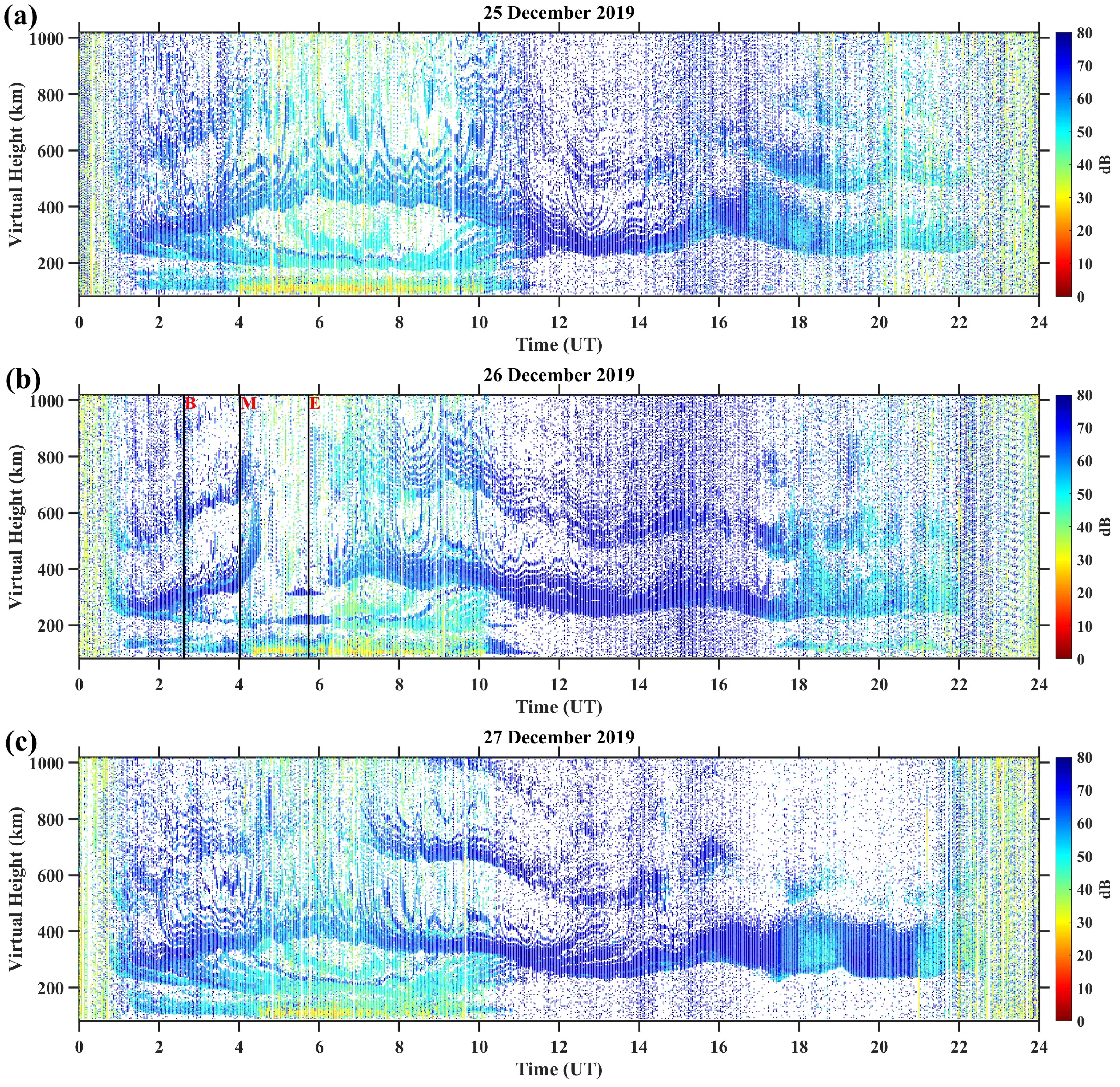
(a)
25 December 2019
Virtual Height (km)
Time (UT)
dB
(b)
26 December 2019
B
M
E
Virtual Height (km)
Time (UT)
dB
(c)
27 December 2019
Virtual Height (km)
Time (UT)
dB

Figure-3(a-d).


(a)
B
M
E
foF2 (MHz)
Time (UT)
25 December 2019
26 December 2019
27 December 2019
(b)
h'F (km)
(c)
foEs (MHz)
(d)
h'Es (km)

Figure-4(a-c).

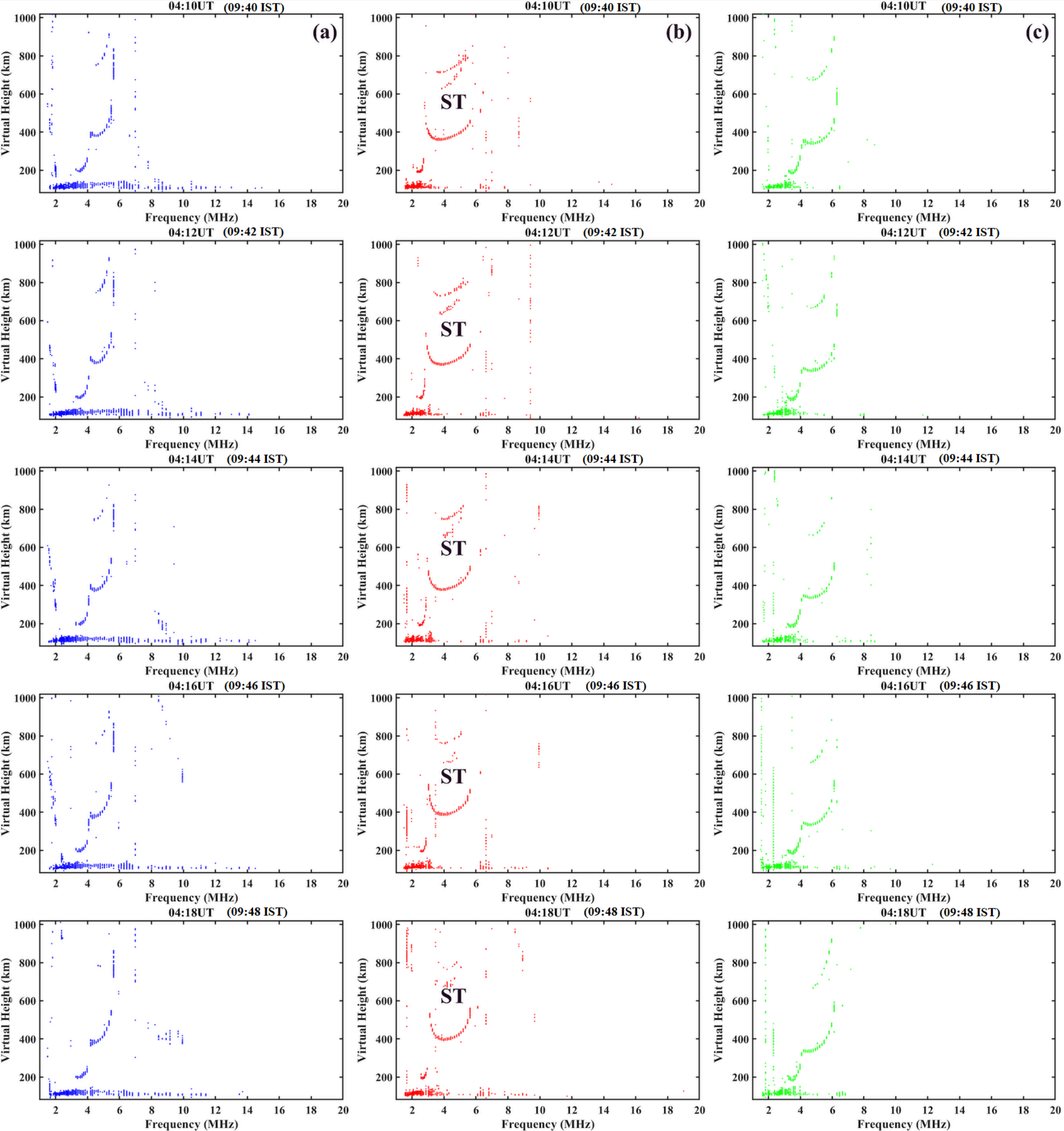

04:10UT (09:40 IST)
(a)
(b)
(c)
ST
04:12UT (09:42 IST)
04:14UT (09:44 IST)
04:16UT (09:46 IST)
04:18UT (09:48 IST)
Virtual Height (km)
Frequency (MHz)

Figure-5(a-d).

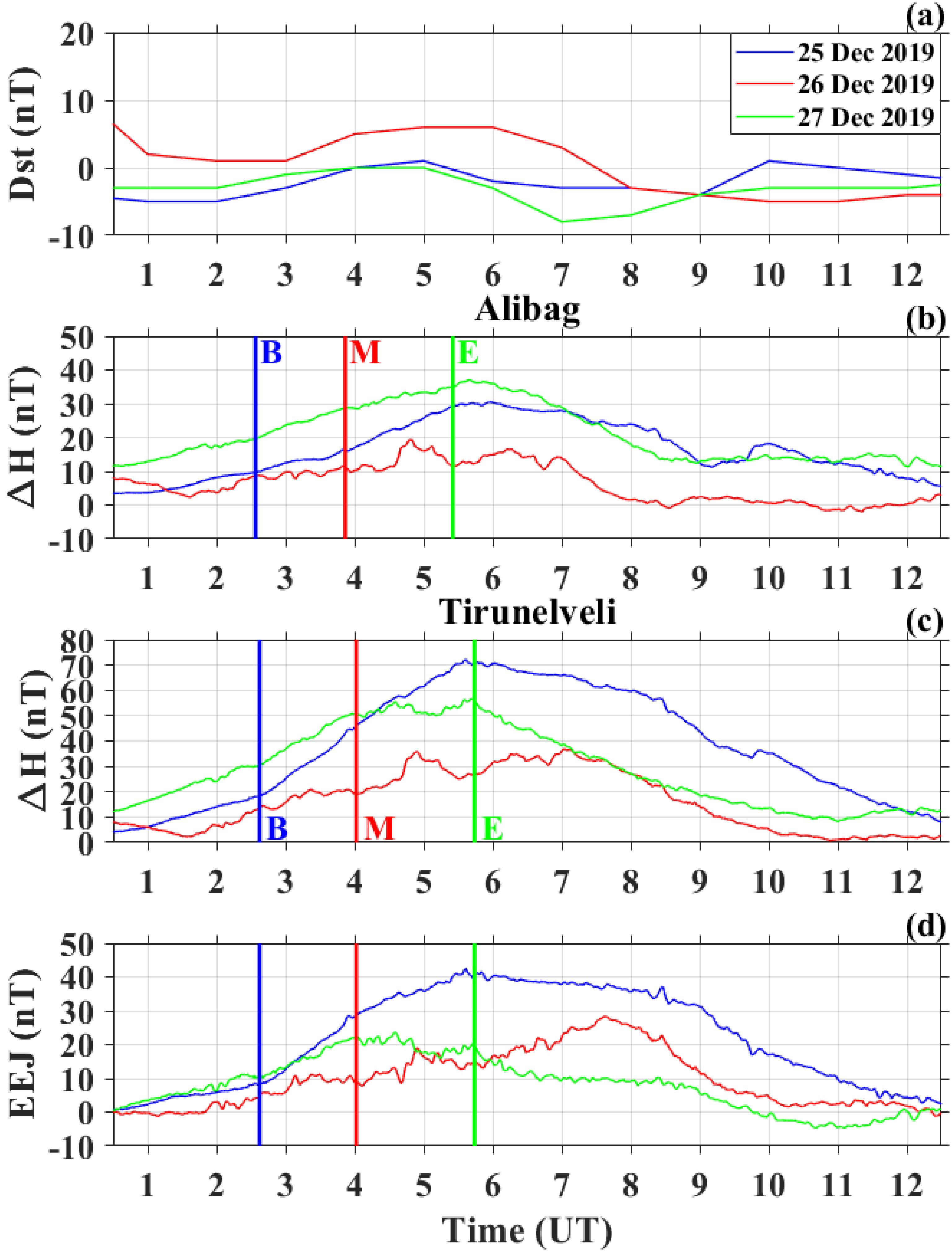
(a)
Dst (nT)
25 Dec 2019
26 Dec 2019
27 Dec 2019
Alibag
(b)
ΔH (nT)
B
M
E
Tirunelveli
(c)
ΔH (nT)
B
M
E
(d)
EEJ (nT)
Time (UT)

Figure-6(a-c).

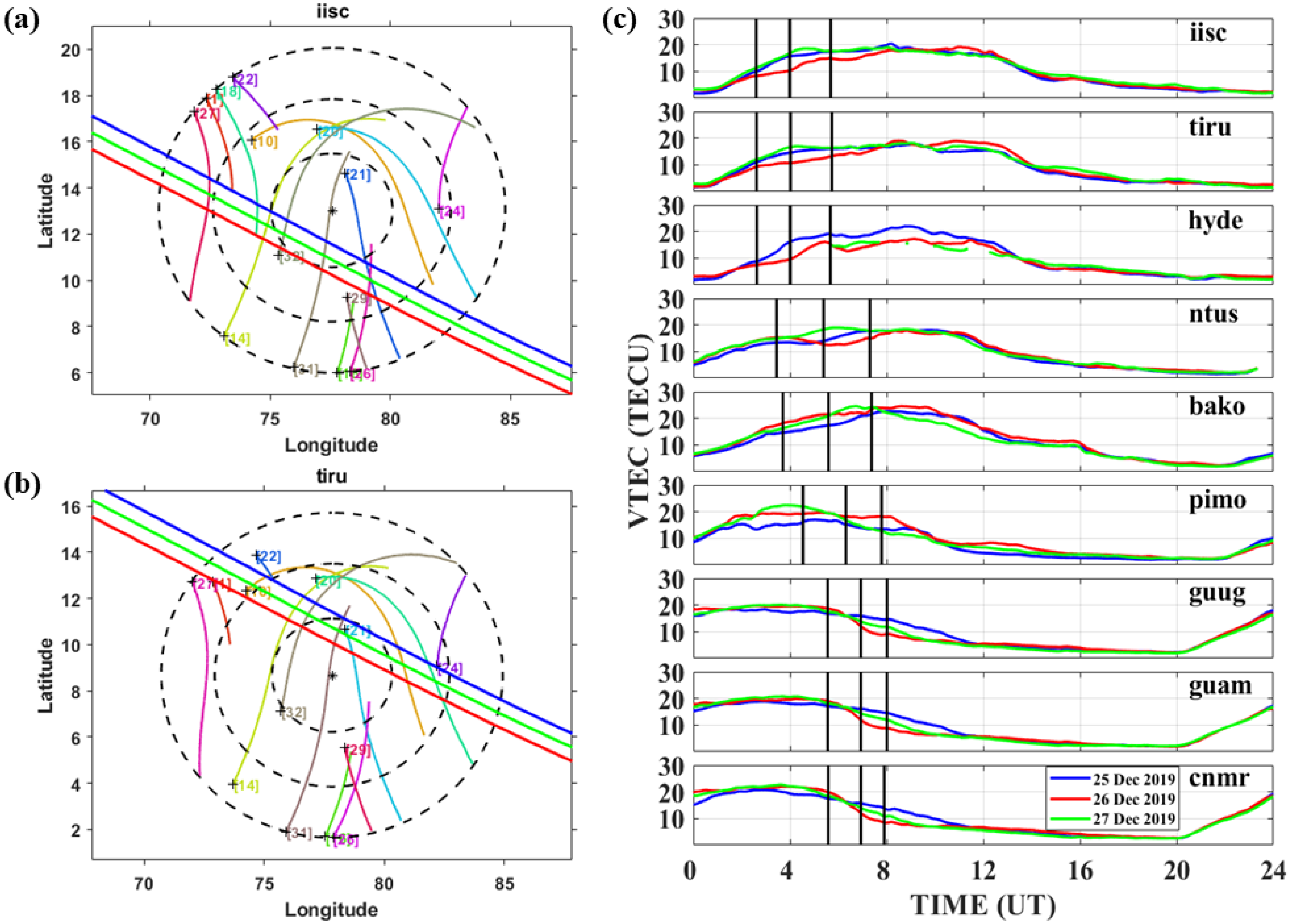
(a)
iisc
Latitude
Longitude
(b)
tiru
Latitude
Longitude
(c)
iisc
tiru
hyde
ntus
bako
pimo
guug
guam
cnmr
VTEC (TECU)
TIME (UT)
25 Dec 2019
26 Dec 2019
27 Dec 2019

Figure-7.

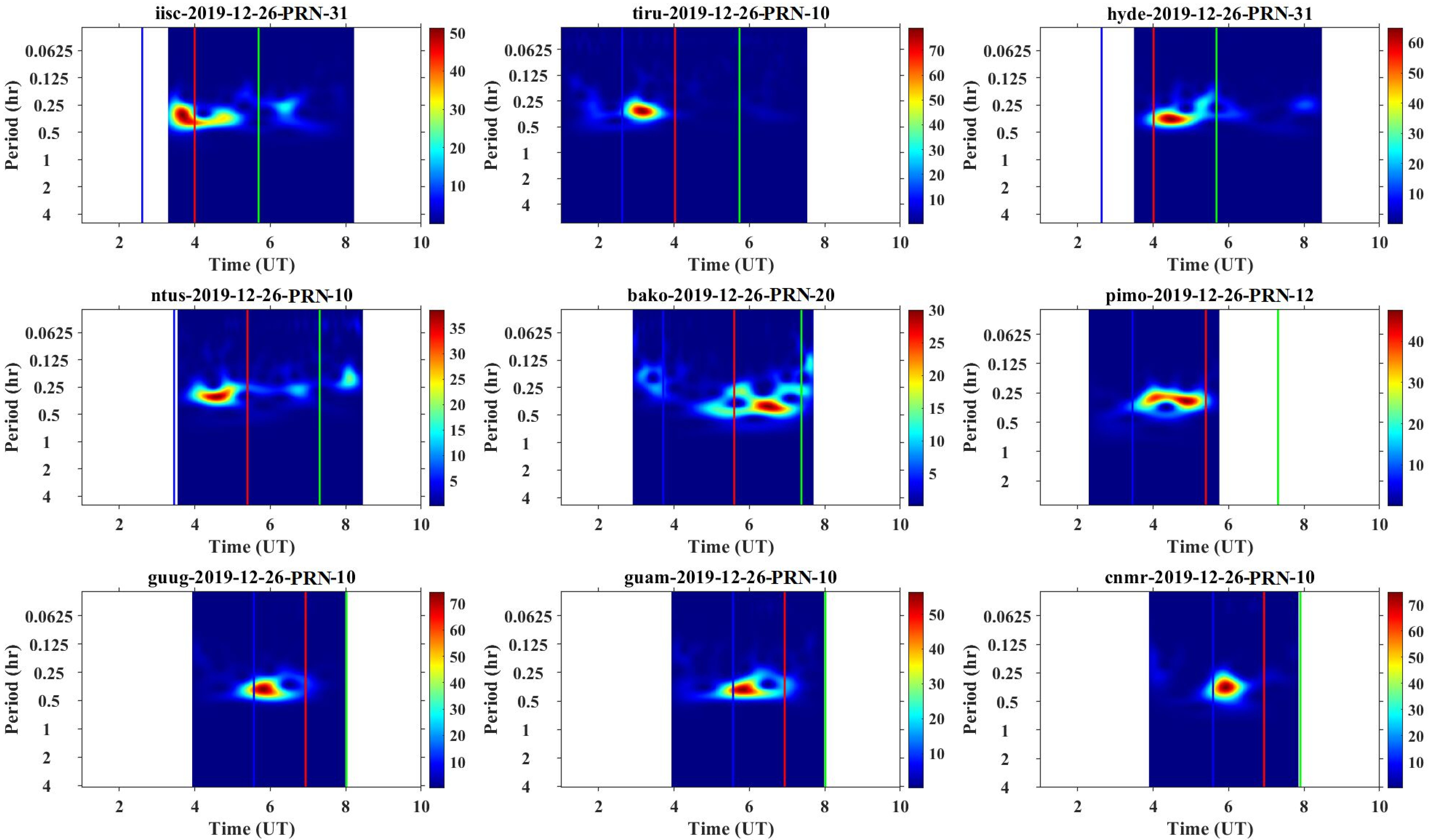
iisc-2019-12-26-PRN-31
tiru-2019-12-26-PRN-10
hyde-2019-12-26-PRN-31
ntus-2019-12-26-PRN-10
bako-2019-12-26-PRN-20
pimo-2019-12-26-PRN-12
guug-2019-12-26-PRN-10
guam-2019-12-26-PRN-10
cnmr-2019-12-26-PRN-10
Period (hr)
Time (UT)

Figure-8(a-c).

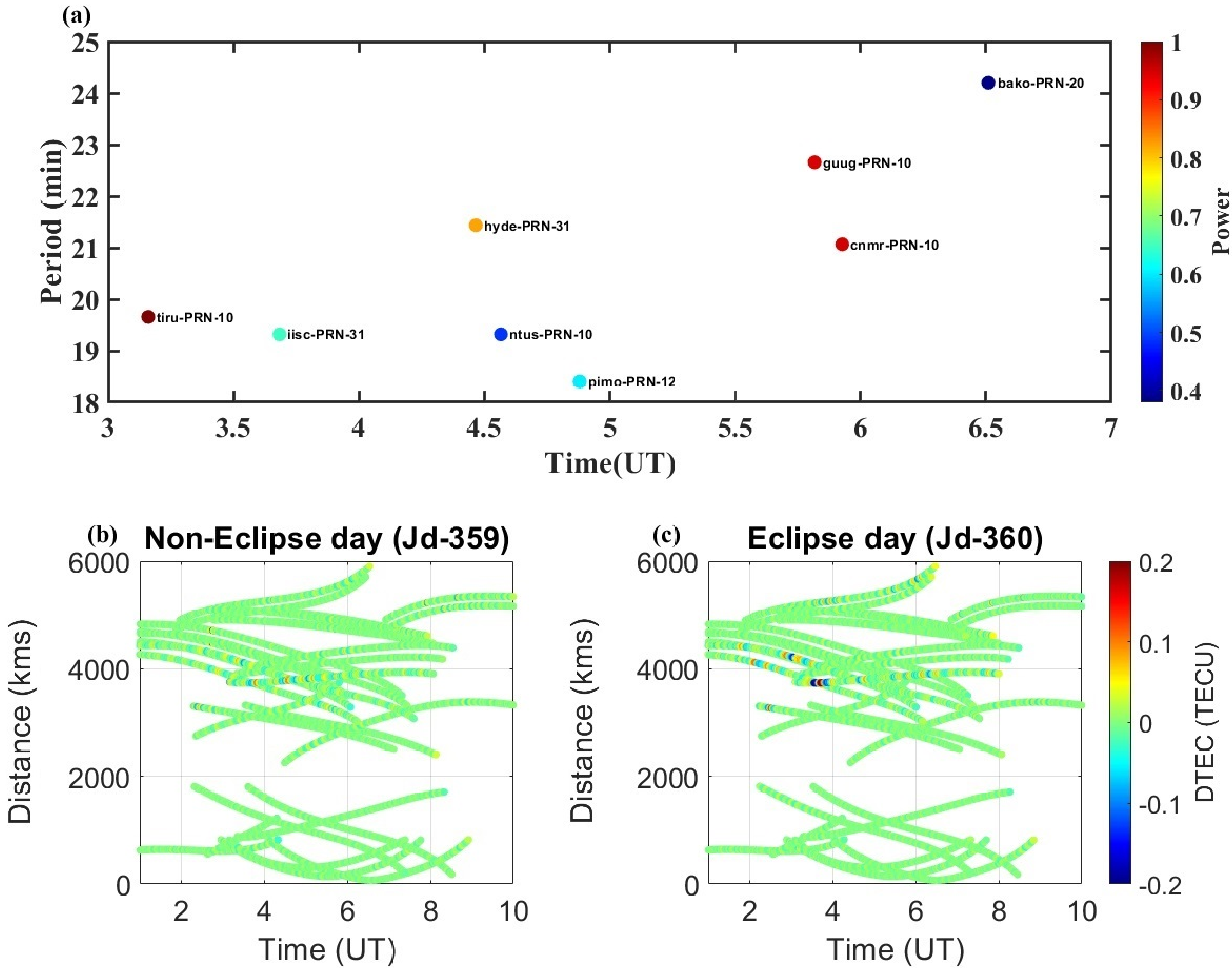

(a)
Period (min)
Time(UT)
Power
tiru-PRN-10
iisc-PRN-31
hyde-PRN-31
ntus-PRN-10
pimo-PRN-12
guug-PRN-10
cnmr-PRN-10
bako-PRN-20
(b)
Non-Eclipse day (Jd-359)
(c)
Eclipse day (Jd-360)
Distance (kms)
Time (UT)
DTEC (TECU)

Figure-9(a-b).

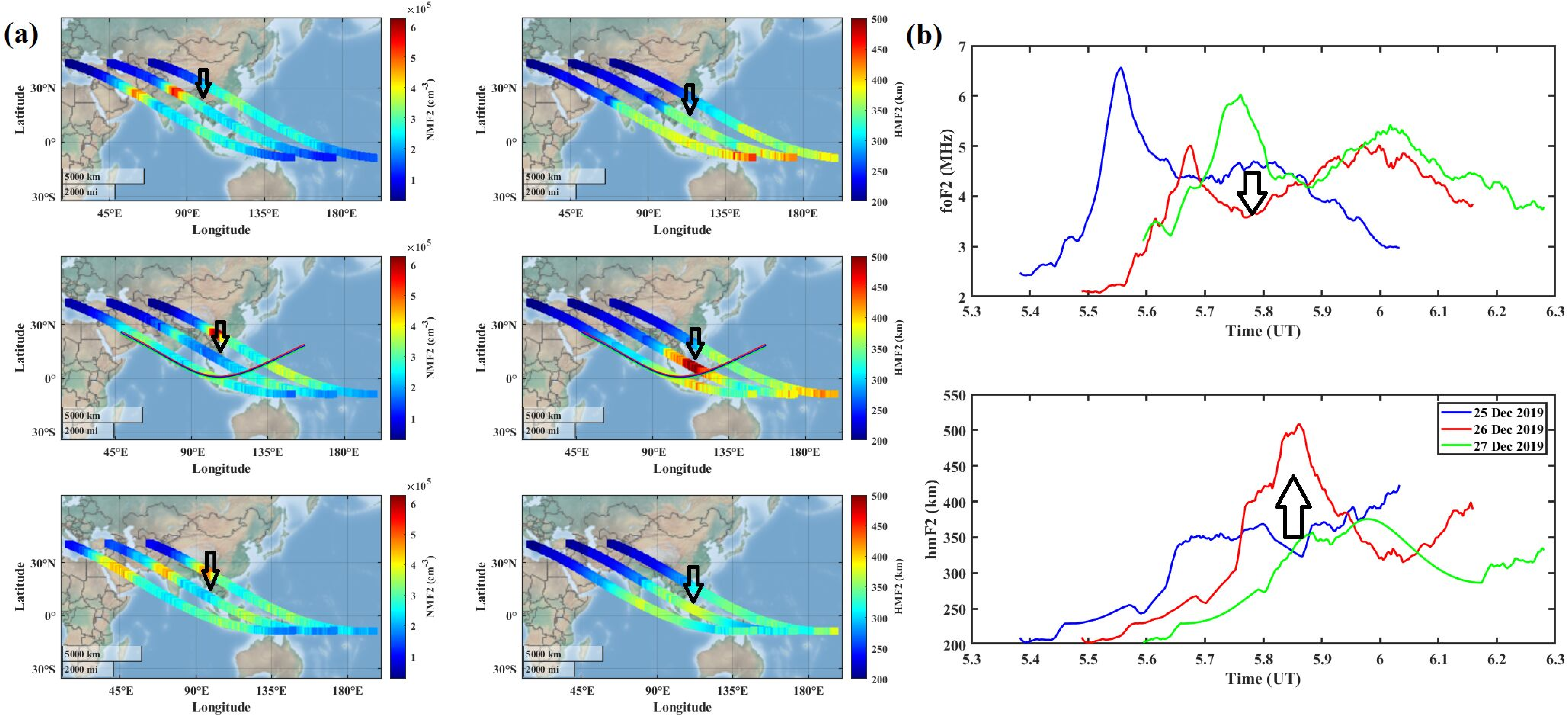
(a)
(b)
Latitude
Longitude
30°N
0°
30°S
45°E
90°E
135°E
180°E
5000 km
2000 mi
NMF2 (cm^{-3})
$\times 10^5$
HMF2 (km)
foF2 (MHz)
hmF2 (km)
Time (UT)
25 Dec 2019
26 Dec 2019
27 Dec 2019

Figure-10(a-e).

25/12/2019
26/12/2019
27/12/2019
(a)
(b)
(c)
Altitude (km)
Time (UT)
Temperature (K)
(d)
25/12/2019 (Time:-05:18 UT-06:01 UT)
26/12/2019 (Time:-05:24 UT-06:09 UT)
27/12/2019 (Time:-05:33 UT-06:16 UT)
Temperature (K)
Temperature difference between eclipse day and control days (ICON)
(e)
Temperature Difference (K)

Figure-11(a-b).

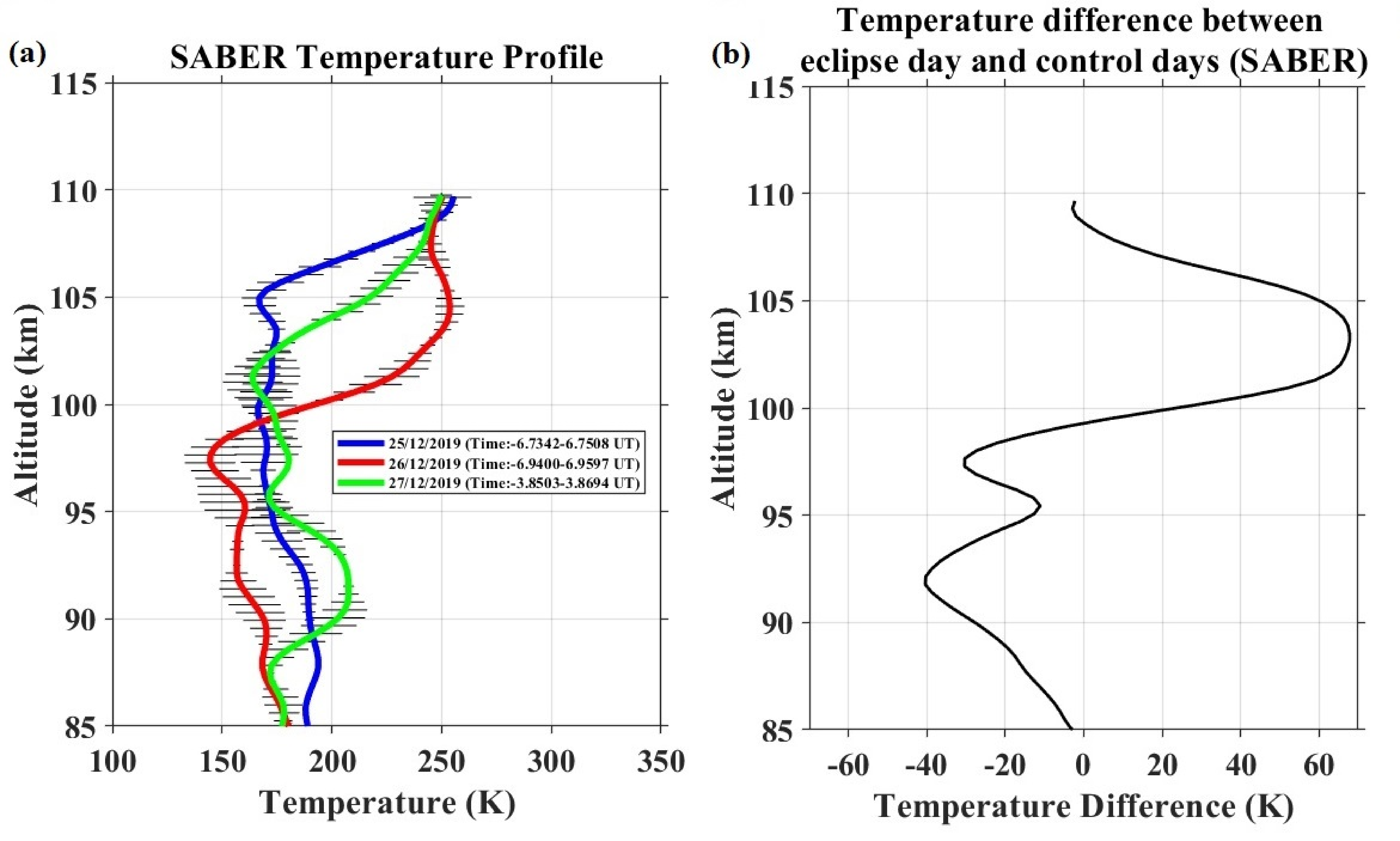
(a)
SABER Temperature Profile
Altitude (km)
Temperature (K)
25/12/2019 (Time:-6.7342-6.7508 UT)
26/12/2019 (Time:-6.9400-6.9597 UT)
27/12/2019 (Time:-3.8503-3.8694 UT)
(b)
Temperature difference between eclipse day and control days (SABER)
Altitude (km)
Temperature Difference (K)